Observations of nearshore groundwater discharge: Kahekili Beach Park submarine springs, Maui, Hawaii

P.W. Swarzenski [a,*], H. Dulai [b], K.D. Kroeger [c], C.G. Smith [d], N. Dimova [a,e], C.D. Storlazzi [a], N.G. Prouty [a], S.B. Gingerich [f], C.R. Glenn [b]

[a] U.S. Geological Survey, 400 Natural Bridges Dr., Santa Cruz, CA 95060, USA
[b] Department of Geology and Geophysics, University of Hawaii, Manoa, Honolulu, HI 96822, USA
[c] U.S. Geological Survey, 384 Woods Hole Road, Woods Hole, MA 02543, USA
[d] U.S. Geological Survey, 600 4th Street South, St. Petersburg, FL 33701, USA
[e] Department of Geological Sciences, University of Alabama, Tuscaloosa, AL 35487, USA
[f] U.S. Geological Survey, 1845 Wasp Blvd., Bldg. 176, Honolulu, HI 96818, USA

ARTICLE INFO

ABSTRACT

Study region: The study region encompasses the nearshore, coastal waters off west Maui, Hawaii. Here abundant groundwater—that carries with it a strong land-based fingerprint—discharges into the coastal waters and over a coral reef.

Study focus: Coastal groundwater discharge is a ubiquitous hydrologic feature that has been shown to impact nearshore ecosystems and material budgets. A unique combined geo-chemical tracer and oceanographic time-series study addressed rates and oceanic forcings of submarine groundwater discharge at a submarine spring site off west Maui, Hawaii.

New hydrological insights for the region: Estimates of submarine groundwater discharge were derived for a primary vent site and surrounding coastal waters off west Maui, Hawaii using an excess ^{222}Rn ($t_{1/2}$ = 3.8 d) mass balance model. Such estimates were complemented with a novel thoron (^{220}Rn, $t_{1/2}$ = 56 s) groundwater discharge tracer application, as well as oceanographic time series and thermal infrared imagery analyses. In combination, this suite of techniques provides new insight into the connectivity of the coastal aquifer with the near-shore ocean and examines the physical drivers of submarine groundwater discharge. Lastly, submarine groundwater discharge derived constituent concentrations were tabulated and compared to surrounding seawater concentrations. Such work has implications for the management of coastal aquifers and downstream nearshore ecosystems that respond to sustained constituent loadings via this submarine route.

1. Introduction

Many islands in the Pacific Ocean are relatively small in size, which makes them especially vulnerable to ocean storms (Dollar and Tribble, 1993; Zhang and Sheng, 2015) as population centers and associated infrastructure align along coastal corridors. Because many of these islands must rely heavily on groundwater as the main source of drinking water (Hunt and Rosa, 2009; Gingerich, 2008; Gingerich and Engott, 2012), the coastal aquifers are particularly sensitive to both marine (i.e.,

* Corresponding author. Fax: +1 831 427 4748.
  E-mail address: pswarzen@usgs.gov (P.W. Swarzenski).

waves, sea-level rise, saltwater intrusion) and terrestrial (pollution, groundwater over-extraction) stressors (Ferguson and Gleeson, 2012; Ketabchi and Behzad, 2015). Groundwater on tropical Pacific Islands is recharged seasonally by precipitation that can be more intensive on the windward side of some high islands (Johnson et al., 2014). This poses challenging intra-island water resources issues (Grubert and Webber, 2015), and as precipitation has also been shown to trend with longer-term climate patterns such as the El Niño-Southern Oscillation (ENSO), climate is thus directly linked to island groundwater resources and sustainability (Strauch et al., 2015).

The sea influences groundwater levels in many coastal aquifers (cf. Cooper et al., 1964) and can affect nearshore sediment transport (Horn, 2006) and biogeochemical transformations (Beck et al., 2007; Rotzoll et al., 2010; Vallejos et al., 2015). The dynamic hydraulic gradient between the sea and coastal groundwater changes in response to wave setup and run up, ocean tides, currents, barometric pressure change, and sea level fluctuations. The tidal signal is attenuated in a coastal aquifer with both distance from shore and depth, and this relation can be used to obtain hydraulic aquifer properties that are essential in long term assessments of water availability and water quality (Rotzoll and Fletcher, 2013). The magnitude and direction of coastal groundwater flow across the seabed can change with the tide; often the greatest submarine groundwater discharge (SGD) rates occur just after low tide when the hydraulic gradients are steepest (Li et al., 1999; Burnett et al., 2001; Swarzenski, 2007; Swarzenski and Izbicki, 2009; Swarzenski et al., 2007; Charette et al., 2008; Moore, 2010; Santos et al., 2012). While SGD can be a ubiquitous, albeit diffuse coastal feature that has been shown to be important in coastal material budgets (Beck et al., 2007; Swarzenski et al., 2007; Slomp and Van Cappellen, 2004; Rodellas et al., 2015a,b; Tovar-Sanchez et al., 2014), some high permeability environments yield abundant submarine springs, where the discharge of coastal groundwater occurs through single or multiple vent features (Swarzenski et al., 2001; Kim et al., 2003; Gonneea et al., 2014; Bakalowicz, 2015; Parra et al., 2015).

Submarine springs have been much less studied than diffuse SGD, yet are important sources of 'new' water and associated constituents to coastal ecosystems, such as coral reefs that typically occur in oligotrophic waters (Swarzenski and Kindinger, 2003; Fleury et al., 2007; Kim et al., 2011). The salinity of discharging groundwater can extend from near fresh to fully marine and may be strongly influenced by the tide and waves (Dimova et al., 2012). Nutrients, trace elements, and other constituents discharged from submarine springs can reveal a direct connection back to the adjacent terrestrial watershed. Groundwater residence times and the biogeochemical nature of a coastal aquifer can vastly transform terrestrial constituents en route to the sea. Thus, submarine springs have been shown to play an important role in the health of coral reefs (Prouty et al., 2016). New studies suggest that sites of sustained SGD, either conveyed by submarine springs or by diffuse flow, may also influence coral bio-erosion rates by altering the pH regime of coastal waters (Vega-Thurber et al., 2014; Evenhuis et al., 2015).

The focus of this paper is to utilize a suite of geochemical tracers and oceanic time-series measurements to examine rates and scales of submarine groundwater discharge at a prominent submarine vent field located just off the coast of west Maui, Hawaii. Here, persistent, focused groundwater discharges into very shallow coastal waters and presents an ideal environment in which to set up in situ experiments on the marine drivers of submarine groundwater discharge and to test the novel application of short-lived ^{220}Rn as a SGD prospecting tool.

2. Study site

The target submarine springs occur in shallow (∼2–3 m) waters just off the coast of west Maui, approximately 6.5 km north of Lahaina in the Kahekili Beach Park area (Fig. 1). The island of Maui is the second largest of the Hawaiian Islands and is composed of two prominent shield volcanoes that influence much of the island's tropical climate (Langenheim and Clague, 1987). Whereas the climate of Maui is characterized by mild and generally uniform temperatures, mean annual precipitation rates vary dramatically with altitude and distance from shore (Gingerich and Engott, 2012). Within just a few kilometers from the coast, mean annual precipitation rates can reach close to 900 cm, as observed on the summit of west Maui at Pu'u Kukui. This is in sharp contrast to precipitation rates that can fall below 50 cm yr^{-1} in the vicinity of the study site (Giambelluca et al., 1986). The geologic features of west Maui have been studied extensively (Stearns and Macdonald, 1942; Langenheim and Clague, 1987). Although Wailuku Basalt is the dominant rock type of west Maui, a veneer of unconsolidated sedimentary deposits may occur along the coast (Fig. 2). These sedimentary deposits and underlying weathered volcanic rocks form a low-permeability confining unit ("caprock"), which restricts the flow of groundwater discharge at the coast (Gingerich and Voss, 2005; Hunt 2007; Gingerich and Engott, 2012; Rotzoll and Fletcher, 2013).

### 2.1. Hydrologic and oceanographic setting

Groundwater in Hawaii occurs in the flank lavas as a thin, freshwater basal lens overlying seawater (Fig. 3), and farther inland, in high-level water bodies impounded by much less permeable dykes (Stearns and Macdonald, 1942; Souza 1981; Gingerich and Voss, 2005; Gingerich, 2008). Groundwater inputs occur as natural recharge from rainfall and infiltration from streambeds, and as artificial recharge from irrigation and anthropogenic wastewater inputs. Natural recharge is greatest in the interior mountains where rainfall is heaviest, but a legacy of large and smaller scale agriculture has dramatically changed rates and magnitude of artificial groundwater recharge in lower elevation, agricultural areas (Shade, 1996; Johnson et al., 2014). Almost 80 years of groundwater recharge for west Maui was estimated by Engott and Vana (2007), who noted dramatic −40% declines in recharge rates during the period 1926–2004. Gingerich and Engott (2012) extended earlier recharge estimates through 2008 and found that as reductions in irrigation and prolonged drought conditions continued for
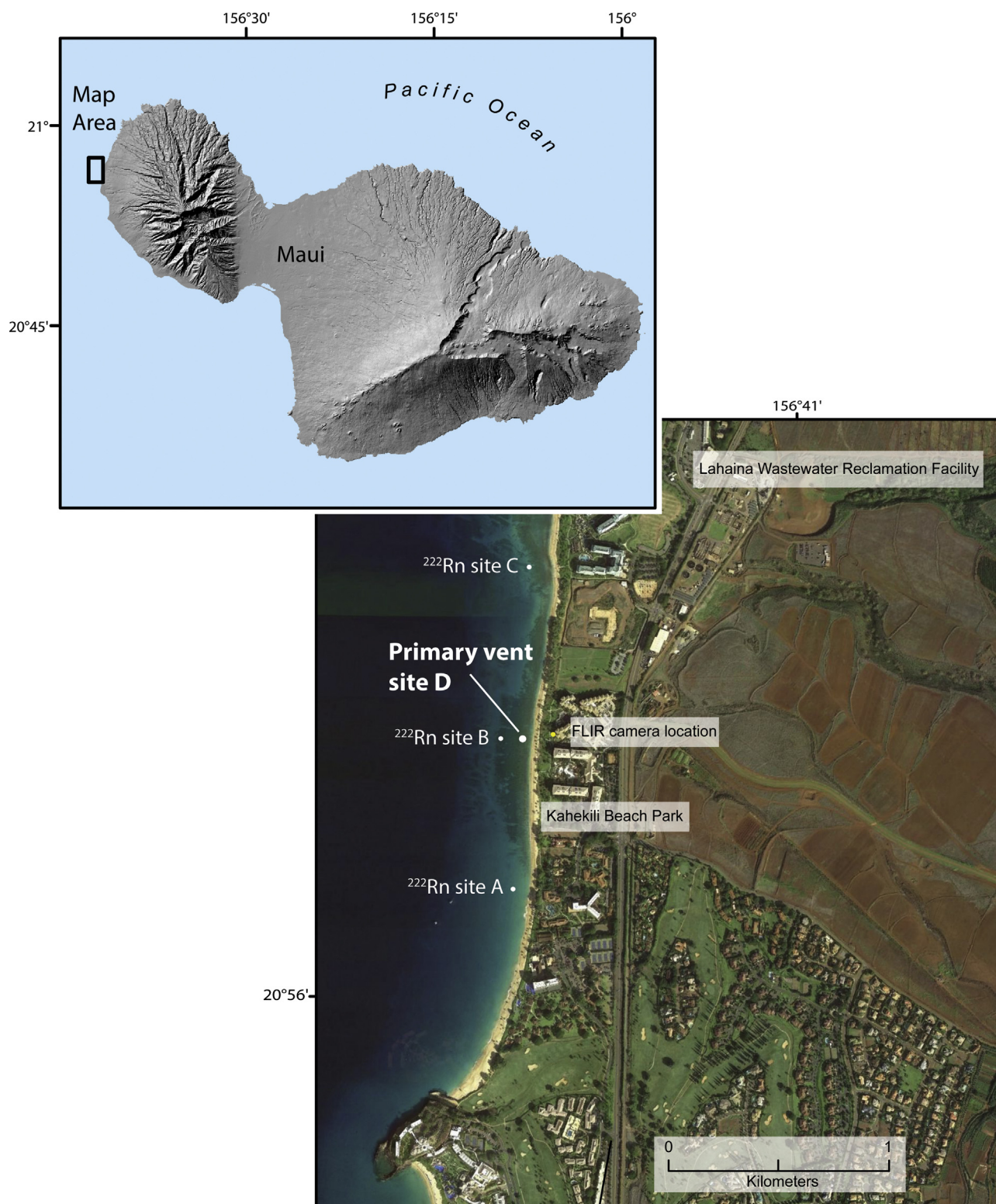
Fig. 1. Location map of the primary vent site off west Maui, Hawaii. Also depicted are the locations of three adjacent ^{222}Rn time-series moorings (A–C), the stationary FLIR camera, and the Lahaina Wastewater Reclamation Facility (LWRF). Note ADCP and ADV instruments and the 4 thermal arrays were all deployed at the primary vent site D. All surface water and vent water sampling was conducted at the primary vent site.
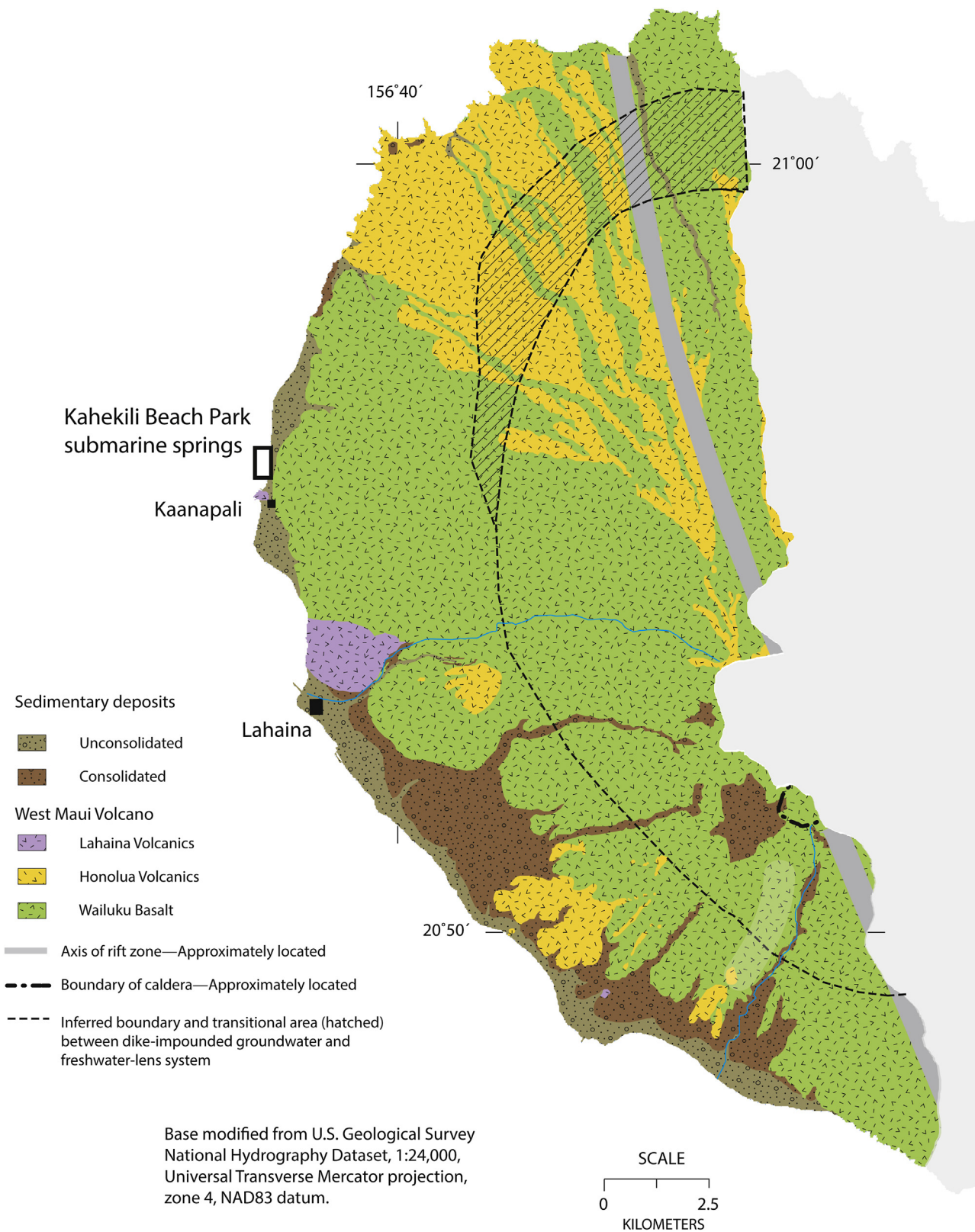
Fig. 2. Simplified surficial geologic map of west Maui, Hawaii, showing the different sedimentary and volcanic deposits (modified from Gingerich and Engott, 2012). The location of Kahekili Beach Park submarine springs are highlighted.
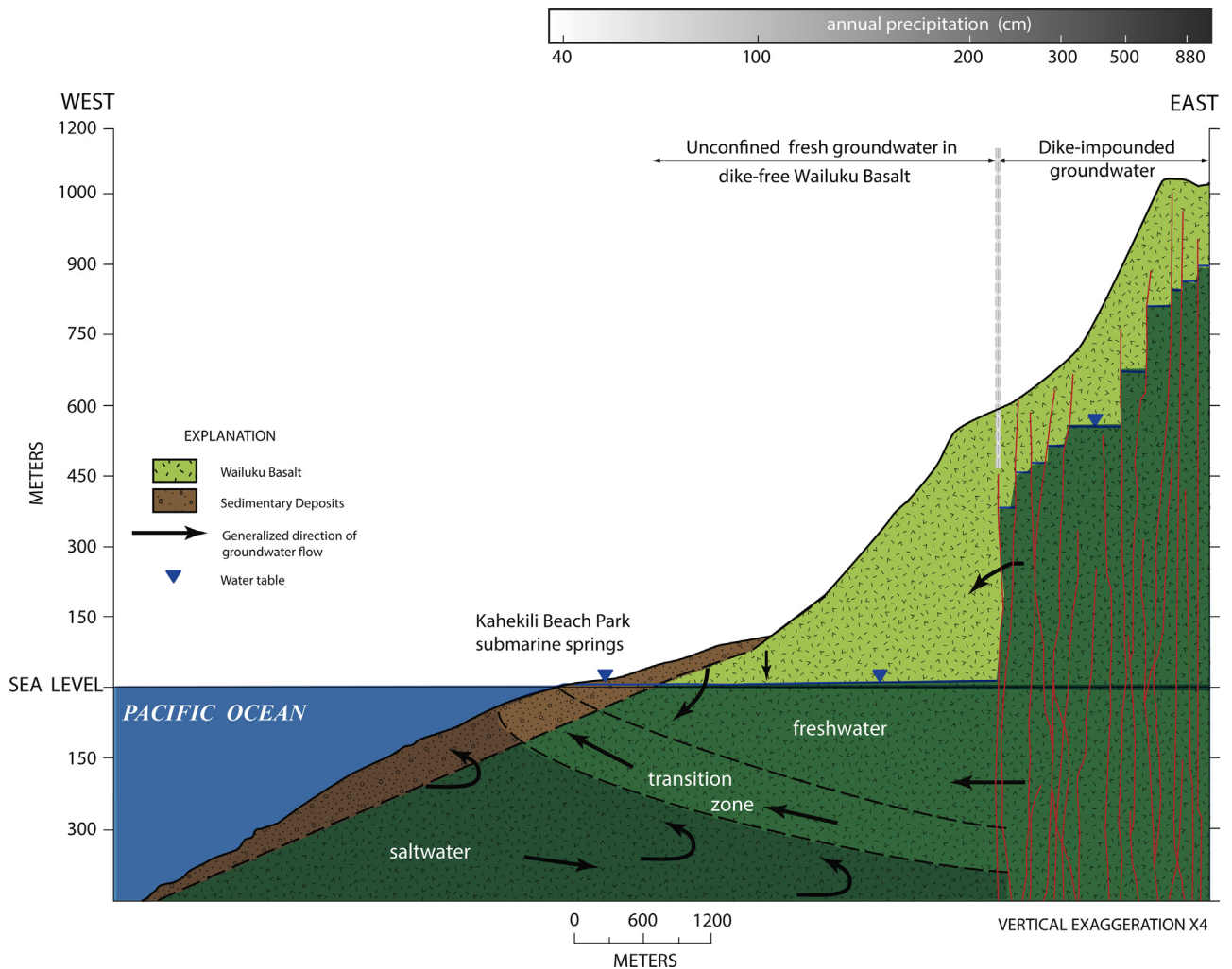
Fig. 3. Simplified hydrogeologic cross-section in the Kaanapali region of west Maui showing precipitation rates, the groundwater table, and likely groundwater transport regimes (modified from Gingerich and Engott, 2012). The location of Kahekili Beach Park submarine springs are highlighted.

west Maui, the combined period 2000–2008 yielded the lowest recharge rates ($\sim 3 \times 10^5$ m^3 d^{-1}) since 1926. For comparison, the total recharge rate for the period 1926–1979 was the highest and close to twice the 2000–2008 rate. The discharge of groundwater occurs as direct extraction from wells, base flow to streams, and seepage to the ocean. While estimates of well withdrawals and base flow contributions to streams are quantifiable components of comprehensive water budget estimates (Souza, 1981; Gingerich and Engott, 2012), direct measurements of coastal groundwater discharge are still rare.

The flow of groundwater to the coast is controlled by hydraulic properties of aquifer material, such as porosity, dispersivity, and hydraulic conductivity and the anisotropy in these parameters. The geology of the area surrounding the study site is dominated by Wailuku Basalt, a band of unconsolidated sediment along the coast, and a small outcrop of Lahaina Volcanics to the south. In general, weathering reduces the permeability of all volcanics through the oxidation of Fe and Mn bearing minerals, thereby reducing porosity and increasing tortuousity. Permeability controls hydraulic conductivity (K), and as the flank lavas exhibit such a high permeability, the water Table gradient (Gingerich and Engott, 2012) in the non-diked area is generally quite small ($\sim$1 cm per 50 m). The regional horizontal hydraulic conductivity of the dike-free volcanic rocks range up to many hundreds of meters per day (Burnham et al., 1977; Rotzoll et al., 2010; Hunt, 2007). On Maui, estimates of the ratio of horizontal to vertical hydraulic conductivity in the water bearing units ranged from 200 to 800 to 1 (Gingerich, 2008). In contrast, Gingerich (2008) had to use values ranging from $\sim$2–5 m d^{-1} for horizontal hydraulic conductivity and $\sim$0.1–0.2 m d^{-1} for vertical hydraulic conductivity of the sedimentary and valley-filling deposits to achieve satisfactory model results.

A MODFLOW groundwater modeling component (Glenn et al., 2013) contributed to the following general controls on regional groundwater transport to the submarine springs of Kahekili Beach Park: (1) density differences between fresh water and seawater, (2) low hydraulic conductivities in the alluvium and weathered basalts associated with modern- and
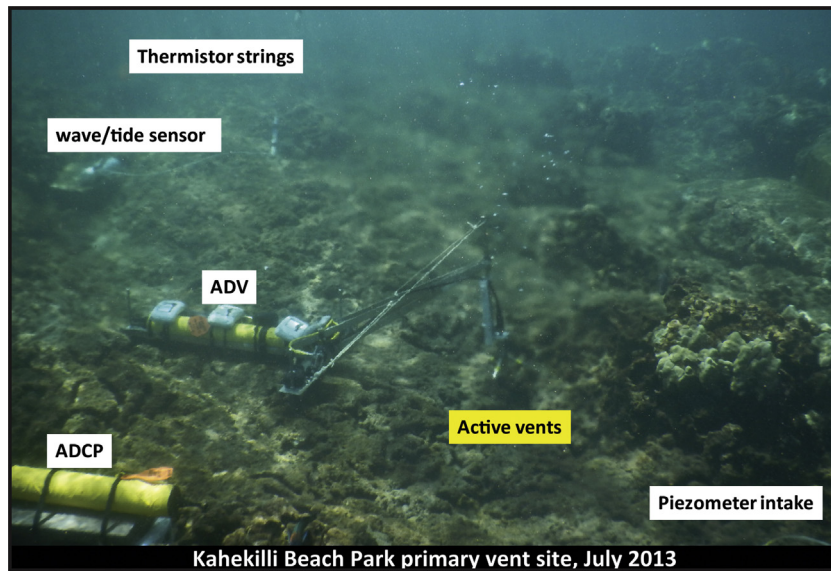
Fig. 4. Photo illustration of the primary vent site D and some of the oceanographic time-series instruments deployed during July 2013. Note the presence of gas bubbles in the water column showing sustained submarine groundwater discharge (SGD) and associated N_2 release. Photo credit: P.W. Swarzenski (USGS).

paleo-channels of the Honokowai Stream form an effective hydraulic barrier to the north both on land and offshore, (3) anisotropy with the dominant axis aligned north–south and perpendicular to the dip of the lava flows. These hydrologic controls combine to convey groundwater in a southwesterly direction towards the submarine springs, as noted by Hunt and Rosa (2009).

Groundwater discharged to the coastal waters is subject to mixing and dispersion by waves and currents. Storlazzi and Field (2008), Storlazzi and Jaffe (2008) and Storlazzi et al. (2006) studied the circulation, residence times, currents, and wave climate in the coastal waters of west Maui. Typically, in shallow (<10 m) water, circulation is influenced by wave- and wind-driven surface currents, while on the outer reef circulation is driven more by tidal forcings. Integrated along-shore current speeds were typically an order of magnitude larger than cross-shore current speeds. Along the 5-m water depth contour line, an observed mean flow of $0.10\,\mathrm{m\,s^{-1}}$ would yield a total water turn over time (replacement time) of just over 3 days, although such an estimate is likely long, as oscillatory tidal flows will enhance these mean flow speeds considerably and reduce turn over times.

2.2. Kahekili Beach Park submarine springs

The studies of Dollar and Andrews (1997), Dollar et al. (1999), and Soicher and Peterson (1997) were among the first to document anomalous nutrient concentration gradients in the coastal waters off Lahaina and inferred an enhanced terrestrial nutrient source (including groundwater) as a likely cause of the water quality degradation. More systematic studies by Smith et al. (2005), Dailer et al. (2008, 2010, 2012) and Hunt and Rosa (2009) used $\delta^{15}N$ in algae and an exhaustive suite of water quality parameters (including pharmaceuticals), respectively, to delineate zones most likely influenced by sewage injectate-impacted groundwater discharge. These and other studies including extensive SCUBA investigations (Glenn et al., 2013) documented the occurrence of multiple submarine vents in the shallow waters north of Kahekili Beach Park that are easy to detect as the discharging water is typically warmer than ambient seawater and rich in N_2 gas bubbles (Glenn et al., 2012), and may create a surface water plume most noticeable at low tide.

A study of submarine groundwater discharge and associated constituent loadings was subsequently conducted in 2010 by Swarzenski et al. (2012, 2013) who developed ^{222}Rn-derived submarine groundwater discharge rates at the primary vent site and in surrounding coastal waters. The Lahaina Wastewater Reclamation Facility (LWRF) is located less than 500 m inland from the coast (Fig. 1) and ~1 km from the primary vent site and uses several injection wells for treated wastewater effluent disposal. A comprehensive suite of tracer studies including tracer dye injections by Glenn et al. (2012, 2013) established that direct hydrologic, geochemical and thermal links existed between the warm, treated wastewaters effluent injected at the LWRF and the groundwater emanating from the submarine vents. Dailer et al. (2012) observed that the coralline rubble and rock surrounding the submarine vents was often coated with a black precipitate, indicative of a Fe- or Mn-oxide deposit. Glenn et al. (2012) subsequently confirmed that these coatings were amorphous MnO_2 that precipitated as low-oxygen groundwater discharges into oxic bottom water. The well-known ability of these Mn-oxides to effectively scavenge (Moon et al., 2003) dissolved Ra (a radiogenic parent of Rn) will prove useful in the application of thoron (^{220}Rn, $t_{1/2} = 56\,s$) as a very short-lived submarine spring discharge 'prospecting' tracer (Section 4.5).
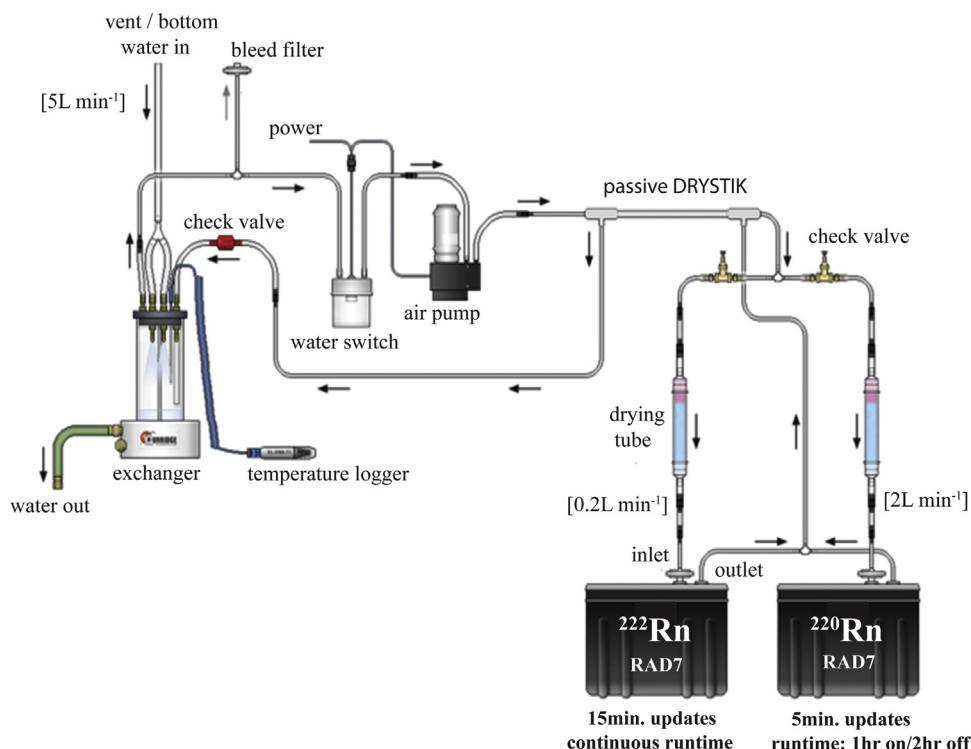
Fig. 5. Schematic diagram showing the optimized RAD7 configuration and sampling setup to analyze for both vent water and bottom water radon ($t_{1/2}$ = 3.8 d) and thoron ($t_{1/2}$ = 56 s). Modified from pers. comm. with Derek Lane-Smith, Durridge, Inc.

Table 1
Nutrient concentrations (μM) in near-shore bottom water and vent groundwater (2010, 2013) at the primary vent site and from the Lahaina wastewater reclamation facility and a suite of upland groundwater production wells (State Well ID: HA2, KP3, KP1, KP2, KP5, and KP4).

	Salinity	Dissolved oxygen (mg L^{-1})	NH$_4^+$ (μM)	Silicate	PO$_4^{3-}$	[NO$_2^-$ + NO$_3^-$]	DIN	DON	TDN
Bottom water (July, 2010)									
Mean	33.8	–	0.07	16.0	0.11	0.20	0.19	6.69	6.88
±	0.2	–	–	5.93	0.06	0.15	0.14	1.20	1.22
Min	33.4	–	0.07	9.48	0.05	0.03	0.03	5.65	5.68
Max	34.1	–	0.07	25.4	0.23	0.40	0.40	9.30	9.48
Vent groundwater (July, 2010)									
Mean	2.8	1.2	0.09	629	12.1	41.3	41.4	10.5	51.9
±	0.8	0.3	0.04	139	0.60	1.24	1.25	1.21	1.78
Min	1.5	0.7	0.03	432	10.0	38.4	38.4	8.81	48.9
Max	4.4	1.9	0.17	814	13.1	42.2	42.3	12.8	54.7
Vent groundwater (July, 2013)									
Mean	7.4	1.0	0.31	581	9.08	72.3	72.6	98.4	148
±	3.7	0.6	0.18	35.8	1.12	15.0	15.0	59.5	56.3
Min	4.2	0.3	0.11	548	8.05	55.6	55.9	17.1	85.7
Max	12.3	1.6	0.60	633	10.5	91.5	91.8	148	240
Lahaina wastewater reclamation facility (LWRF, July 2013)									
Mean	1.0	7.0	31.3	521	26.0	270.4	301.8	77.6	379.4
±	–	–	6.30	24.3	1.56	37.8	44.1	34.4	78.6
Upland production wells (July 2013)									
Mean	0.4	8.9	0.08	693	3.32	70.6	70.7	4.37	75.1
±	0.2	0.2	0.04	89.8	1.46	39.2	39.2	4.12	43.0
Min	0.2	8.7	0.01	576	1.79	34.1	34.1	0.77	35.7
Max	0.6	9.1	0.12	806	5.61	124	124	11.8	137

Table 2
Trace element concentrations (nM) in bottom water and vent groundwater (2010) at the primary vent site.

Bottom water						
	Mo (nM)	Ba	V	U	Cr	Mn
Mean	106	30.2	39.2	11.0	59.6	112
±	2.9	0.30	5.80	0.3	60.8	98.0
Min	98.0	29.0	32.0	10.0	3.0	7.0
Max	110	30.0	51.0	11.0	178.0	320
Vent groundwater						
Mean	45.3	17.2	291	0.8	82.8	12,220
±	7.50	3.5	44.4	0.2	64.3	1,990
Min	30.0	11.0	200	0.6	1.0	8,355
Max	54.0	22.0	348	1.0	204	14,500

3. Methods

Initial field work at the Kahekili Beach Park submarine vent site was conducted 11–16, July 2010 and then revisited during 7–12 July 2013 to assess the marine forcings on SGD rates using a suite of oceanographic instruments and a combination of both radon and thoron as SGD tracers (Fig. 1). Details of the sampling techniques used during the 2010 field campaign are summarized in Swarzenski et al. (2012).

The 2013 fieldwork built on previous field experiments that utilized ^{222}Rn mass balance calculations to derive SGD rates at the primary vent site and in adjacent coastal waters. Briefly, a 3–4 tidal cycle time-series of ^{222}Rn activities in vent and coastal water was used to calculate SGD rates (Swarzenski et al., 2012). A suite of water samples was also collected from the discharging vent and bottom water using trace element clean sample collection techniques. These water samples were analyzed for dissolved nutrients (NH_4^+, Si, PO_4^{3-}, [$NO_3^- + NO_2^-$]), dissolved inorganic nitrogen (DIN), dissolved organic nitrogen (DON), total dissolved nitrogen (TDN), and select dissolved trace elements (Mo, Ba, V, U, Cr, and Mn) following trace element clean sampling methods described in Swarzenski et al. (2007, 2009, 2012). Nutrients were analyzed at the Woods Hole Oceanographic Institution (WHOI) nutrient laboratory via flow injection analysis for NH_4^+, Si, PO_4^{3-}, and [$NO_3^- + NO_2^-$], with precisions of 0.6%, 0.8%, 0.9%, and 0.3% relative standard deviations, respectively. Select trace element (Mo, Ba, Re, V, and U) concentrations were determined by high-resolution inductively coupled plasma mass spectrometry (HR-ICP–MS) at the University of Southern Mississippi (USM Center for Trace Analysis).

For the 2013 field work, an inflatable boat was carefully anchored above the most prominent vent site D and was used as a mooring platform to house an array of instruments and detectors (Fig. 1). Because of the inherent difficulties in sampling the discharge of any submarine spring before the groundwater discharge plume gets overwhelmed with ambient seawater, a piezometer point was carefully inserted directly into the most active vent. A Teflon sampling tube was connected to this piezometer and routed to the moored inflatable. By continuously sampling from this piezometer, vent water with salinities as low as 3 were obtained (ambient seawater salinities were ~34–35).

During the 2013 deployment, the following oceanographic instruments were deployed in the shallow waters of the study site (Figs. 1 and 4): an upward-looking 2-MHz Nortek Aquadopp acoustic Doppler current profiler (ADCP), a downward-looking 6 MHz Nortek Vector acoustic Doppler velocimeter (ADV) that was focused on the most active vent site, and four vertical thermistor arrays that each consisted of 3 RBR Solo temperature probes tethered to a subsurface float and anchored to the seabed. One temperature array was positioned directly above the vent site and the remaining three were positioned at equal distances from the center array.

The ADCP collected data in 0.25-m bins from the seafloor up to the surface for 250 s at 2 Hz every 5 min. to allow calculation of tidal height (m), mean current speeds (m s^{-1}), and mean current directions (°True). Directional wave data were recorded for 1024 s at 2 Hz every hour; these data included wave height (m), wave period (s), and mean wave direction (°True). The ADV recorded high-precision, three-dimensional eastward, northward, and upward velocity point measurements and pressure in hourly bursts of 1024 measurements at 2 Hz (17.1 min). The water pressure bursts were used to calculate the spectral wave energy. The water column thermistor arrays each consisted of 3 RBR Solo (temperature) sensors (depth from the water surface = −0.3 m, −0.5 m, and −1.3 m) and set to sample at a frequency of 5 s. On the center, vent thermistor array, an additional RBR Duo (pressure and temperature) was placed on the seabed anchor and also set to a sampling frequency of 5 s.

On the inflatable boat, three RAD7s radon detectors were setup to continuously sample for vent water and bottom water ^{222}Rn ($t_{1/2}$ = 3.8 d), and vent water ^{220}Rn ($t_{1/2}$ = 56 s). The following setup was optimized for both ^{222}Rn and ^{220}Rn analyses (pers. comm. Dr. Derek Lane-Smith, Durridge, INC.). Briefly, vent water was continuously pumped using a 12 V peristaltic pump into an high-flow air/water exchanger fitted with a continuous temperature data logger (Fig. 5). Air from the exchanger was directed through a water trap, an auxiliary variable-speed air pump, and a passive Drystik before being split into two regulated lines that were directed into the ^{222}Rn and ^{220}Rn RAD7s. The ^{222}Rn RAD7 was set up to acquire data at a 15 min. sampling frequency, in continuous run time mode, and with an air flow rate of 0.2 L min^{-1}. In contrast, the ^{220}Rn RAD7 was set up with a 5 min. sampling frequency, an intermittent run time (1 h on/2 h off/1 h on, etc) using an air flow rate = 2 L min^{-1}.
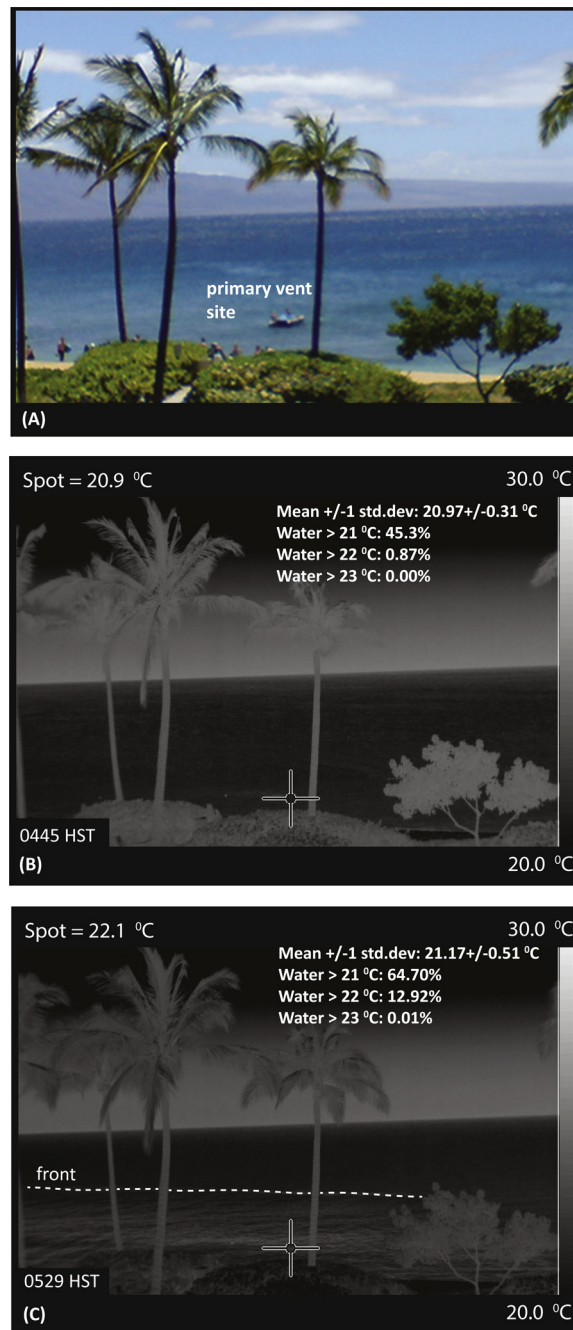
Fig. 6. Examples of true color (A) and night time uncorrected thermal infrared images (B, C) obtained from a stationary, hand-held FLIR camera positioned about 100 m away from the primary vent site.

Airflow rates were precisely controlled using dedicated needle valves and flow meters. The exhaust air stream from both RAD7s was merged before being routed into the passive Drystik and then back to the exchanger. 'Bottom' water ^{222}Rn was continuously sampled at a depth of -0.5 m from the surface using a 12 V bilge pump and a dedicated RAD7 (15 min. sampling rate) and exchanger. Rn-222 was quantified using the counts in Window A from the α-emitting radon daughter ^{218}Po ($t_{1/2} = 3.10$ min), while ^{220}Rn was analyzed using the counts in Window B from the α-emitting radon daughter ^{216}Po ($t_{1/2} = 0.15$ s). The salinity and temperature of the vent water and bottom water were continuously recorded using calibrated YSI multi-probes.

The groundwater emanating from the west Maui submarine springs is warmer than ambient seawater (Swarzenski et al., 2012; Glenn et al., 2012, 2013). This is unlike many other coastal groundwater sites where the discharging water is usually

cooler than ambient seawater (Johnson et al., 2008; Kelly et al., 2013). To capitalize on this thermal anomaly, a fixed-position, thermal infrared (TIR) camera was used to delineate the size and shape of the SGD-influenced surface plume over several tidal cycles (Fig. 1). TIR imagery was obtained using a FLIR model SC660 handheld thermal imaging camera during the same July 2013 sampling campaign. The camera was positioned on an ocean-facing, third story hotel balcony about 100 m inland and an intervelometer captured imagery every 60 s. The FLIR camera has a resolution of 640×480 pixels, a spectral range of 7.5–13 μm, a sensitivity of 30 mK at 30 °C, and a minimum accuracy of ± 1 °C.

4. Results and discussion

4.1. Nutrients and trace element concentrations

Select nutrient and trace element concentrations were analyzed in both the primary vent water and ambient seawater to assess the scale of terrestrial inputs into nearshore seawater. Tables 1 and 2 present contrasting nutrient and trace element concentrations of a suite of samples collected during July 2010, 2013 of submarine vent- and adjacent bottom-water, respectively. In general, the groundwater discharging from the primary vent site had a lower pH (<7.5) than ambient coastal water (∼8.0). In 2010, the mean salinity of the discharging vent water was 2.8 ± 0.8, while the mean bottom water salinity was 33.8 ± 0.2. The mean dissolved oxygen concentration of the discharging vent water was consistently hypoxic at 1.2 ± 0.3 mg L^{-1}. Dissolved nutrient concentrations of the discharging vent water were also quite different than observed in bottom water. For example, the mean Si concentration in discharging vent water of 629 ± 139 μM was ∼39 times as enriched relative to the bottom water mean concentration of 16.0 ± 5.9 μM. Similarly, the discharging vent water was more than 100 times (PO_4^{3-}), 200 times ($[NO_2^- + NO_3^-]$ and DIN = dissolved inorganic nitrogen), 1.5 times (DON = dissolved organic nitrogen), and 7.5 times (TDN = total dissolved nitrogen) as enriched relative to bottom water concentrations. The suite of trace elements also exhibited pronounced differences in the discharging vent water and in bottom water, with concentrations reflecting the low dissolved oxygen content of the discharging groundwater. For example, the mean dissolved Mn concentration in discharging vent water of $12,220 \pm 1990$ nM was enriched more than 100 times over the mean bottom water mean concentration of 112 ± 98 nM. Vanadium was also 7.4 times elevated in the discharging vent water (mean V concentration = 291 ± 44.4 nM), while Mo (0.4 times), Ba (0.6 times), and U (0.1 times) were all more enriched in the bottom waters than in the reducing vent water.

Nutrient concentrations were also measured in July 2013 in the discharging vent water, the LWRF injectate, and in five upland production wells removed from any marine influence. While the mean dissolved oxygen concentrations in vent water were similar for 2013 (1.0 ± 0.6) and 2010 (1.2 ± 0.3), the mean salinity of the vent water was about 2.5 times higher in 2013 (7.4 ± 3.7) than in 2010. The mean nutrient concentrations observed in 2010 and 2013 were generally on the same order of magnitude, with the notable exception of DON, which was enriched about 9-fold during 2013. The LWRF injectate samples were enriched 0.9 times (Si), 2.5 times (PO_4^{3-}), 4.8 times ($[NO_2^- + NO_3^-]$), 5.3 (DIN), 1.4 times (DON), and 3.8 times (TDN) relative to combined mean 2010 and 2013 vent water concentrations. For comparison, the upland production well samples were all oxygenated (mean dissolved oxygen concentration 8.9 ± 0.2 mg L^{-1}), and while Si, $[NO_2^- + NO_3^-]$, and DIN concentrations were similar to the mean combined 2010 and 2013 vent water concentrations, DON and PO_4^{3-} concentrations were markedly lower (0.31 times and 0.08 times), respectively.

The findings of Glenn et al. (2012, 2013) indicate that while there are several hundred small vent features in the shallow (<3 m) waters off Kahekili Beach Park, larger, non-ephemeral submarine springs are rarer and can be grouped into two N-S trending clusters. Dye tracer experiments and geochemical mixing models suggest that up to 96% (mean 62%) of the discharging vent water can be sourced back to the LWRF injectate, although redox- and microbially-mediated biogeochemical transformation reactions within the coastal aquifer modify constituent loads as they are transported to the sea. These reactions reduce nitrogen via denitrification (Dailer et al., 2010, 2012; Hunt and Rosa, 2009; Glenn et al., 2012, 2013) and also enrich phosphate (Swarzenski et al., 2012; Glenn et al., 2013), introducing some uncertainty into mixing-model calculations.

4.2. Thermal IR imagery

As the discharging groundwater temperature at the primary submarine vent site is consistently warmer and more buoyant than ambient seawater, the thermal signature of the surface water over time can provide an estimate of the groundwater-influenced surface plume size and shape. A total of 2580 true color and infrared images of the primary vent site were collected identically during the July 2013 fieldwork. Only night-time infrared data were used in assessments of SGD plume dynamics to minimize the effects of solar heating. Without applying corrections to address the camera viewing angle (in this case ∼75°) that affect how well an absolute water temperature can be inferred from TIR data (Duarte et al., 2006), each TIR image was consistently processed to eliminate any intra-image variability and then grouped into user-defined temperature bins to assess change over time.

As shown in Fig. 6B and C, the uncorrected FLIR data can be used in this manner to assess the relative change in surface water temperature over time. Such analysis provides an easy way to evaluate change in the surface water temperature regime over time or tidal stage. Based on the these simple methods, a strong thermal front was most prominent during the falling tide and reveals the width of a band of warm surface water most impacted from the discharging submarine spring;
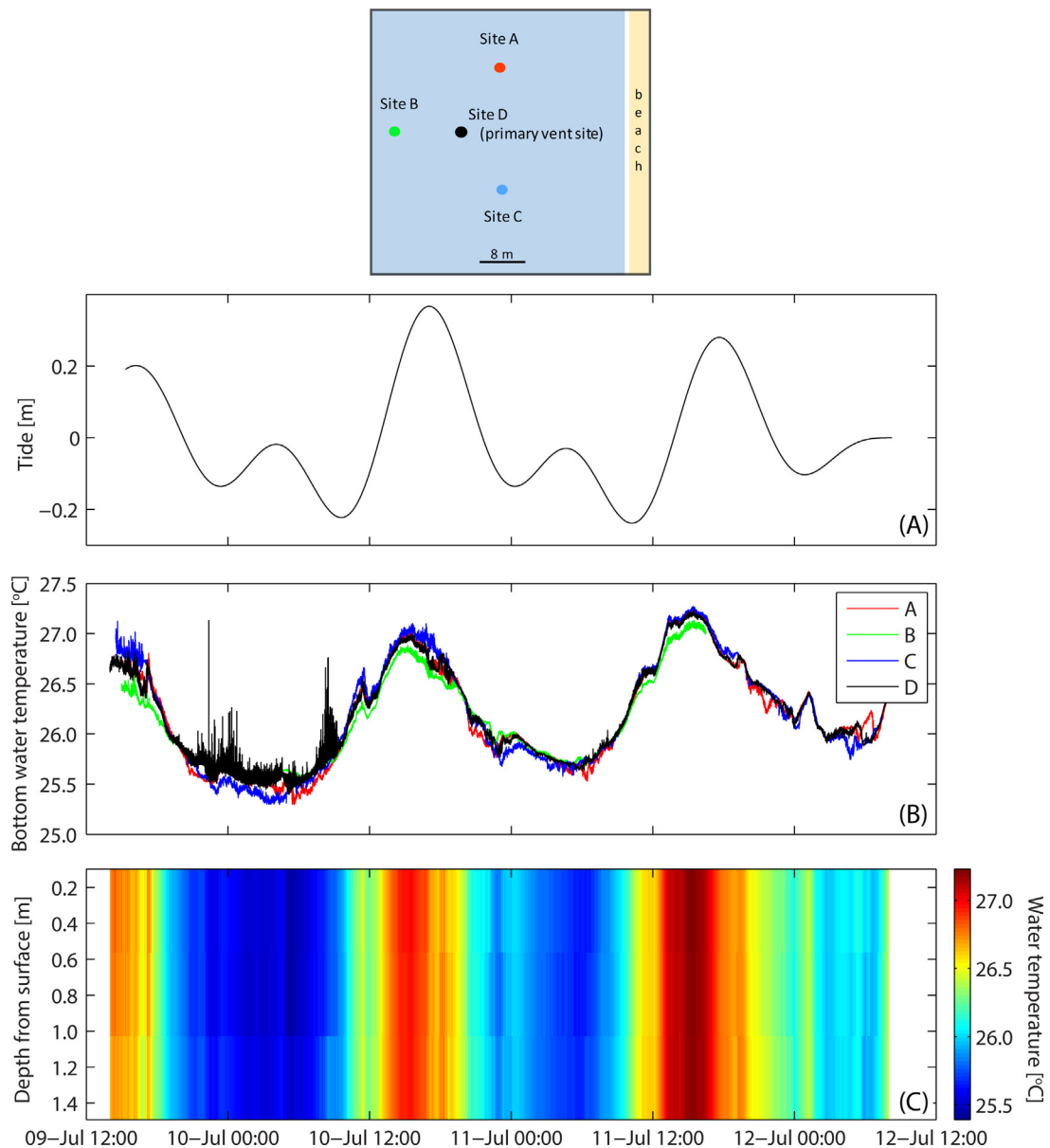
Fig. 7. Results from the four thermistor arrays that were located at the primary vent site (array D) as well as in the surrounding water column (array A–C). (A) shows the water level (tide), (B) shows the time-series, bottom water temperature record for each of the four arrays, and (C) shows a 2D image of the vertical temperature distribution at the primary vent site (array D). Sustained, anomalous warm bottom water temperatures were picked up by array D, and likely reflect a hydrologic response to a large swell event that just preceded the observational record.

the areal extent of waters greater than 22 °C and 23 °C each increased by more than an order of magnitude during the falling tide. While Johnson et al. (2008) and Kelly et al. (2013) have clearly shown the utility of airborne IR imagery to identify and study sites of sustained surface water SGD expressions over large water bodies, the use of handheld TIR cameras shows promise as a surveying tool to identify SGD sites and can also provide a rapid, cost-effective perspective on the presence, scales, and dynamics of SGD (Duarte et al., 2006).

4.3. Thermistor arrays

Heat carried by groundwater can be a powerful hydrologic tracer (Anderson, 2005) to study both infiltration and discharge rates (Taniguchi, 1993; Banks et al., 1996; Constantz et al., 2002; Niswonger and Prudic, 2003; Taniguchi et al., 2003). The four thermistor arrays deployed in the shallow waters at the primary vent site were not used to obtain rates of hydrologic exchange—the water column is much too shallow and dynamic for such derivations—but rather to assess to what extent
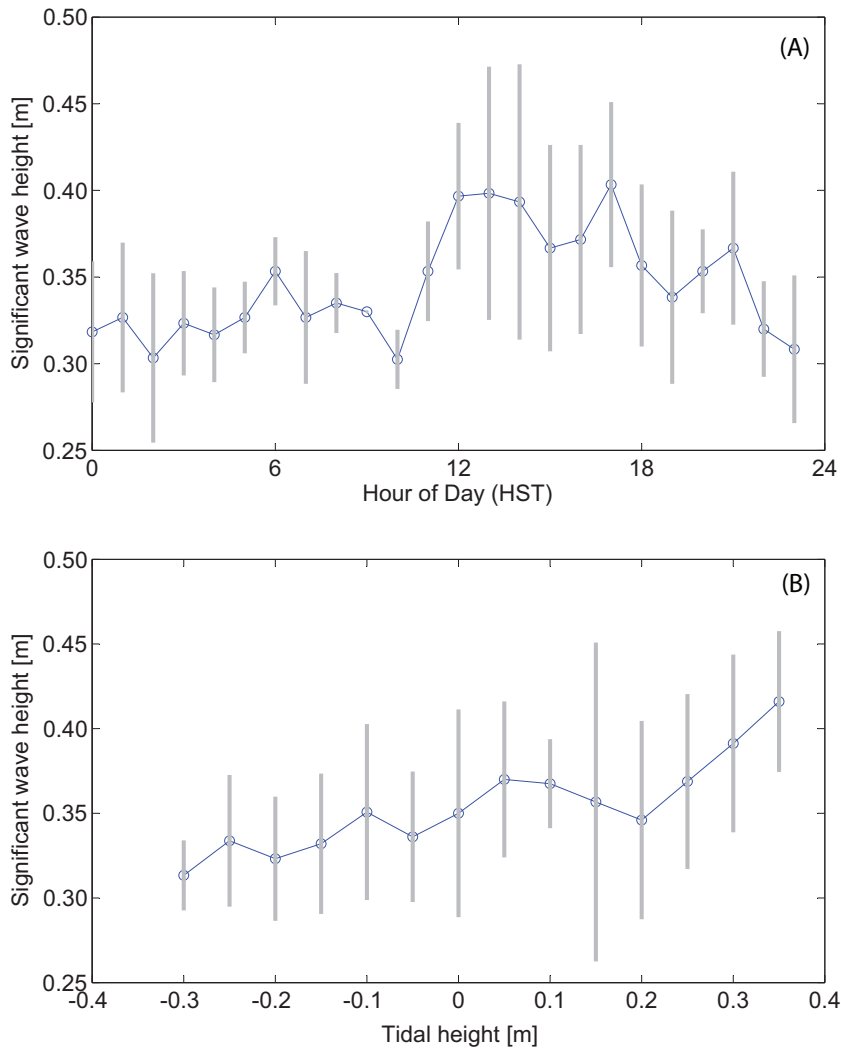
Fig. 8. Wave conditions during the experiment. (A) Mean and standard deviations of significant wave height (Hs) for hours of the day (HST), and (B) mean and standard deviations of significant wave height versus as a function of tidal height. Note that waves were largest in the afternoon due to sea breezes and during higher tides, demonstrating that this area is depth-limited for the wave heights and periods observed during the study.

the thermal signature of the discharging groundwater plume is visible in the adjacent water column. Scales of mixing can be easily assessed from these temperature arrays. Temperatures at all three depths of each thermistor array ranged from a low of about 25.5 °C to just above 27.0 °C, and showed little vertical structure at any of the four arrays (Fig. 7). Pronounced anomalies in the temperature record were expressed primarily in the bottom waters at the primary vent site (site D), where unusual spikes in temperature were most pronounced during a falling tide. These thermal anomalies lasted for a ~12-h period starting at 2100 on 9 July 2013, and capture the response of the hydrologic system at the primary vent site to a large northeasterly swell event that occurred just before the sampling event rather than just ambient tidal forcings per se.

4.4. Winds and waves

The tides of west Maui are mixed, semi-diurnal and the tidal range during the deployment period in July, 2013 was ~0.66 m. Circulation patterns in the shallow coastal waters off west Maui are driven by wave- and wind-driven surface flows (Storlazzi et al., 2003, 2006). During the July 2013 sampling period, wind speeds were generally <5 m s^{-1} in the mornings and late evenings and peaked above 10 m s^{-1} in the early afternoons. The wind direction during this time of year was predominantly southerly. Mean significant wave heights generally decreased from 0.5 m at the beginning of the experiment to 0.3 m by the end of the study (Fig. 8), but were modulated by the sea breeze and tide, with slightly larger waves in the afternoon when the winds were the strongest and the tides were higher, which allowed for larger depth-limited waves. The dominant wave period was ~14.5 s for much of time series and gradually decreased to ~13.5 s by 12 July. The near-seabed and near-surface current speeds ranged up to 0.19 m s^{-1} and 0.23 m s^{-1}, with mean values of 0.06 and 0.07 m s^{-1}, respectively. A
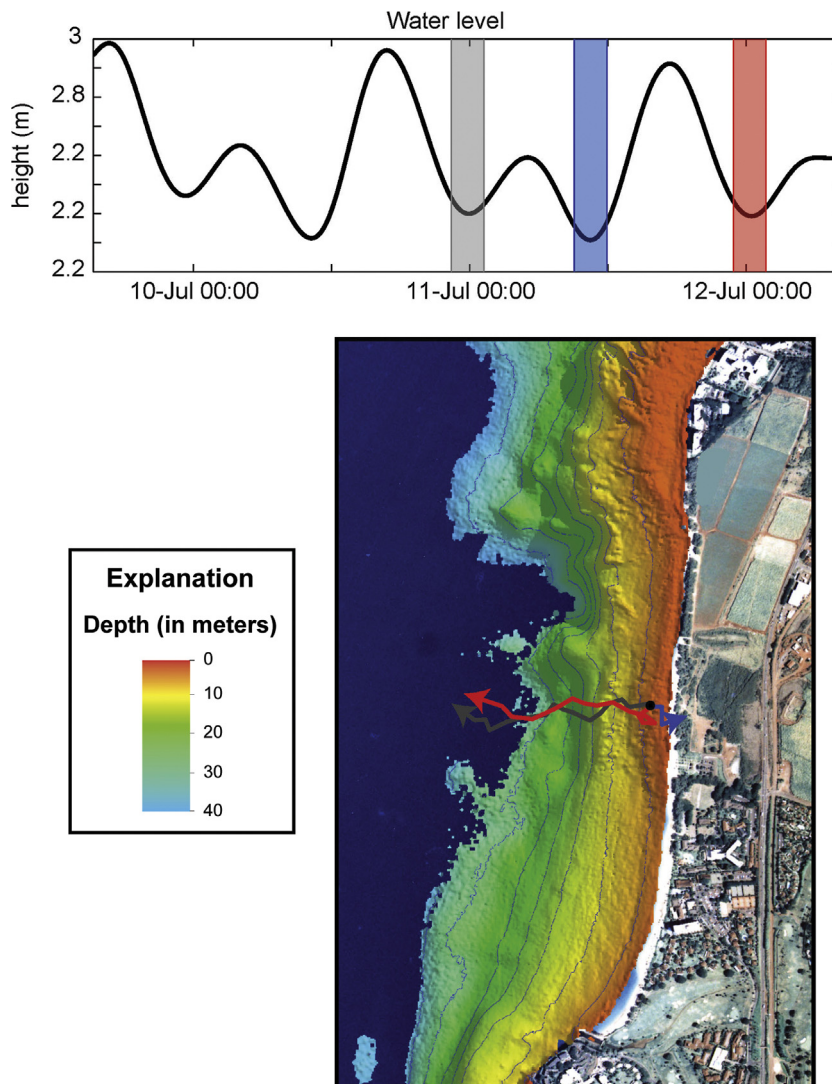
Fig. 9. Map showing ADCP-derived 3-h cumulative surface water flows during around successive low tide events at the primary vent site D. The cumulative flow vectors are colored relative to the date and time (top panel). Note that the current velocities and thus cumulative flow distances were greater and oriented offshore when the tide dropped from the higher high to the higher low, whereas they were smaller and oriented onshore when the tide dropped from the lower high to the lower low.

low-tide snapshot (when groundwater discharge rates are greatest) revealed that surface currents were strong and directed offshore during the largest decrease in water depth when the tide dropped from higher high to higher low tide, resulting in net derived cumulative flow carrying the groundwater-laden surface waters offshore (Fig. 9). During the smaller decrease in water depth when the tide dropped from the lower high to the lower low, however, the currents and resulting mean flow was weak and oriented onshore. As submarine groundwater discharge rates were generally highest just after low tide events (see Section 4.5), such results provide estimates into how the freshened SGD plume mixes with ambient seawater and is transported away from the primary vent site. Such transport processes have implications to coral health, as both constituent loadings and contact or residence times affect exposure.

The 2 Hz ADV water pressure and vertical velocity records were analyzed to evaluate the effects of tides and waves on vent discharge. During high tides when waves were also larger, the change in water column depth (i.e., pressure) was greatest, and the vent showed a larger dynamic response ($0.011 \, \mathrm{m \, s^{-1}}$ upward $\mathrm{dbar^{-1}}$) than during lower tides, when the waves were smaller ($0.007 \, \mathrm{m \, s^{-1}}$ upward $\mathrm{dbar^{-1}}$); these relationships were significant above the 95th percentile. This greater dynamic response to waves at high tide occurred despite the $2 \pm 5 \, \mathrm{mm \, s^{-1}}$ faster vertical flow out of the vent at low tide than at high tide. Together, these show the influence of water levels and hydraulic gradients—both at wave and tidal frequencies—on submarine groundwater discharge at the vent site.
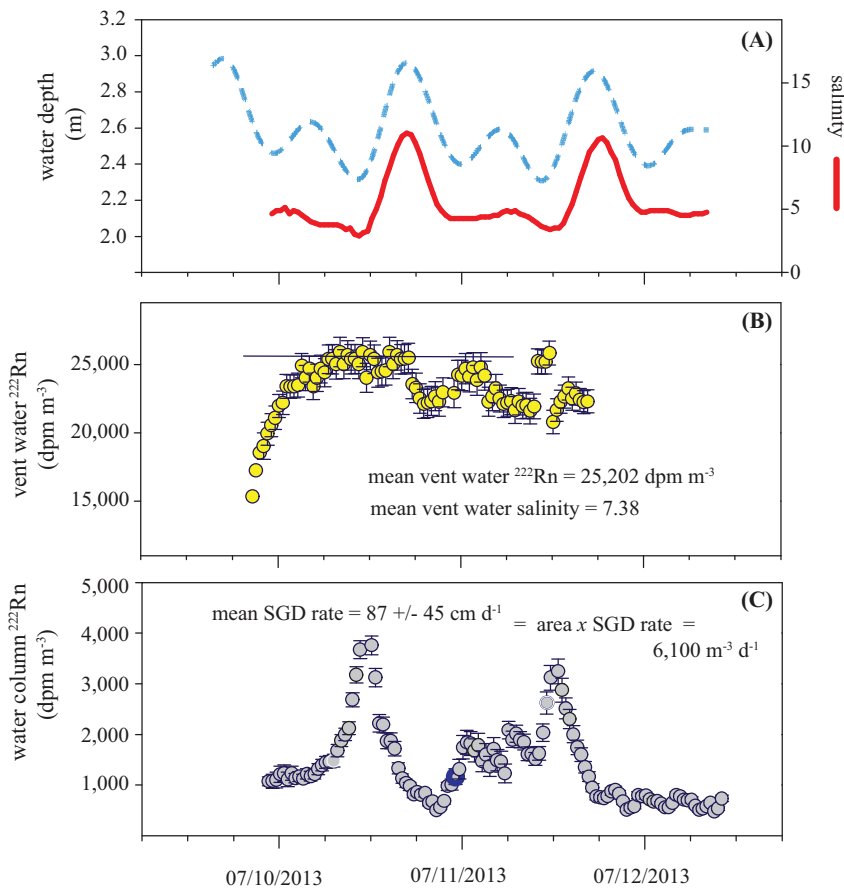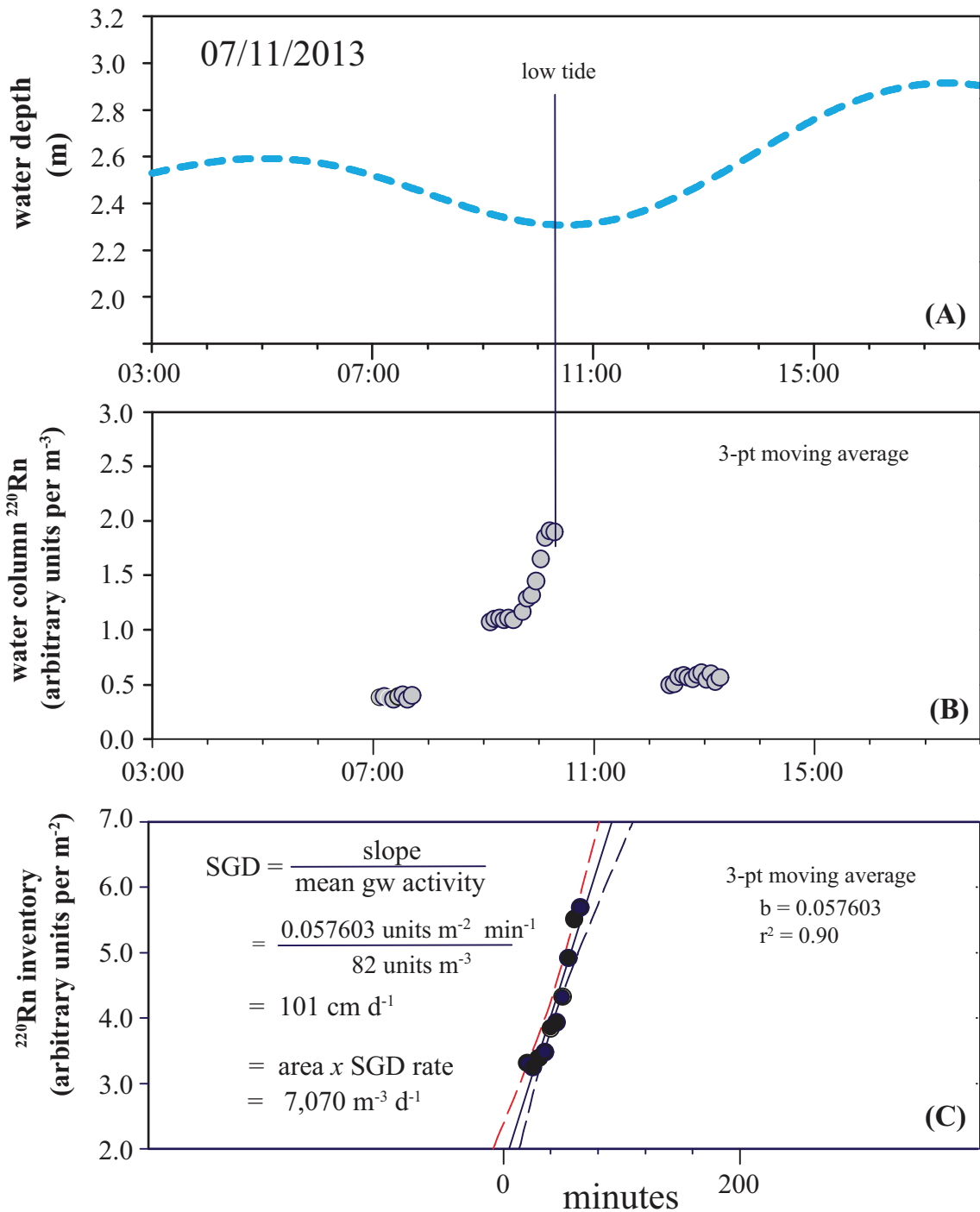
Fig. 10. (A) 2013 time-series record of the tide and vent groundwater salinity, (B) vent groundwater ^{222}Rn activities. A mean vent water ^{222}Rn activity of 25,200 dpm m^{-3} is used in the derivation of SGD rates at the primary vent site. (C) time-series water column ^{222}Rn activities recorded over several tidal cycles. A calculated ^{222}Rn-derived SGD rate of 87 ± 45 cm d^{-1} multiplied by the area (70 m × 100 m; Glenn et al., 2013) most influenced by the cluster of discharging vents surrounding the primary vent site studied here yields a volumetric SGD rate of 6,100 m^3 d^{-1}.

4.5. Radon and thoron as submarine groundwater spring tracers

Radon-222 is a powerful naturally occurring tracer to study water transport processes, including combined (fresh and saltwater) submarine groundwater discharge (Burnett and Dulaiova, 2003; Burnett et al., 2003, 2007a). The utility of the isotope is that it has a short half-life ($t_{1/2} = 3.8$ days) that is closely matched to many hydrologic time scales of interest (~ 4 times $t_{1/2}$), is a noble gas and so chemically inert, and is usually much enriched in groundwater relative to surface water (Swarzenski, 2007; Charette et al., 2008). Recent advances in the analyses of ^{222}Rn have been simplified by a commercially available RAD7 Rn-in-air monitor and a simple water-air exchanger that enables one to calculate the aqueous Rn activity from the measured air activity using the temperature dependent partitioning coefficient (Burnett et al., 2001; Burnett and Dulaiova, 2003; Dulaiova et al., 2006; Swarzenski et al., 2006; Schubert et al., 2012). This advance in instrumentation has reinvigorated interest in ^{222}Rn as a hydrologic tracer in lakes (Cartwright and Gilfedder, 2015), rivers (Atkinson et al., 2015; Ortega et al., 2015), and the coastal ocean (cf. Rodellas et al., 2015a,b).

During July 2010, a groundwater and bottom water ^{222}Rn time series was conducted at the primary vent site D (Swarzenski et al., 2012) and also at three additional water column sites surrounding the primary vent site (Fig. 1). The three distal ^{222}Rn mooring sites were chosen based on bottom sediment type as well as distance away from the primary vent site D. Site A targeted sand deposits south of the primary vent site, site B was located seaward of the primary vent site to discern the offshore extent of the active submarine vents, and site C was located north of the primary vent site and targeted volcanic outcrops (Swarzenski et al., 2012). Rn-222 in the discharging vent site D showed a clear inverse relation with the tide. A mean ^{222}Rn activity in the discharging vent groundwater of 27,000 dpm m^{-3} was used in mass balance calculations to derive SGD rates at all four surface water sites for July 2010. This groundwater endmember value agrees well with similar values as reported in Peterson et al. (2009). By developing a mass balance for excess ^{222}Rn in the surface waters, the following SGD rates were derived: at the primary vent site D the SGD rate was highest (mean = 55 ± 56 cm d^{-1}); at the peripheral sites A, B, and C, Rn-derived SGD rates were 21 ± 36, 30 ± 41, and 22 ± 41 cm d^{-1}, respectively. As site B may be influenced by

Fig. 11. (A) 2013 time-series record of the tide, (B) bottom water ^{220}Rn activities (arbitrary units per m^{-3}) and (C) using ^{220}Rn inventories (arbitrary units per m^{-2}) to derive an SGD rate of 101 cm d^{-1}. Multiplying this ^{220}Rn-derived SGD rate by the area most impacted by the submarine vents (7,000 m^2; Glenn et al., 2013) yields a volumetric SGD rate of 7,070 m^3 d^{-1}.

tide-dependent offshore transport of surface water, the heightened SGD signal observed at this site may be attributed in part to Rn-rich vent water advected into deeper water.

Acknowledging the assumptions inherent in such a ^{222}Rn model that accounted for atmospheric radon evasion, *in-situ* production from its radiogenic parent ^{226}Ra, coastal mixing and tidal exchange (Burnett and Dulaiova, 2003; Burnett et al., 2001, 2003, 2006, 2007a; Dulaiova et al., 2006; Swarzenski et al., 2006, 2007, 2009), such results confirm that groundwater discharge was most pronounced at the primary vent site, but was still detectable at the distal ^{222}Rn time series site B (Fig. 1).

This implies that groundwater discharge is not just constrained to the shallow vent site D, but as modeling has also shown (Gingerich and Engott, 2012), is much more regional in scale.

For the July 2013 field operations, ^{222}Rn time-series measurements were again conducted in the groundwater and bottom waters at the primary vent site to obtain combined SGD rates. Radon measurements were also expanded to also include the very short-lived tracer thoron, ^{220}Rn ($t_{1/2} = 56$ s). The premise for attempting to utilize ^{220}Rn as an event submarine groundwater tracer is two-fold; Glenn et al. (2012) documented the occurrence of Mn-oxide coatings on submarine vent rocks which are well known to effectively concentrate parent Ra isotopes and thus provide an enriched source of localized Rn isotopes, and ^{222}Rn activities are considerably elevated in the discharging submarine groundwater (consistently above 25,000 dpm m^{-3} in waters with salinity <4) so the groundwater here is indeed rich in U/Th-series weathering products.

A 2013 time-series record of the tide versus vent groundwater salinities at site D shows that salinity measurements were consistently below 5 except during high tide events, when the salinities increased to above 12 and revealed tidally-forced seawater infiltration (Fig. 10a) . A mean groundwater (Fig. 10b) ^{222}Rn activity of 25,200 dpm m^{-3} and water-column ^{222}Rn activities that showed clear peaks during low tide events (Fig. 10c) were used in the derivation of SGD rates. A ^{222}Rn-derived SGD rate of 87 ± 45 cm d^{-1} multiplied by the area (70 m $\times$ 100 m; Glenn et al., 2013) most influenced by the cluster of discharging vents surrounding the primary vent site yields a volumetric SGD rate of 6,100 m^3 d^{-1}. This value compares favorably with the total Rn-derived SGD rates obtained by Glenn et al. (2013) who also inferred that ~3/4 of their total SGD rate (6,300 m^3 d^{-1}) at this site consisted of fresh water. Both the 2010 and 2013 ^{222}Rn data illustrate that this groundwater tracer, that was enriched at least 6-fold in vent groundwater relative to bottom waters, is effective at quantifying groundwater discharge rates in the submarine vent field off Kahekili Beach Park. Such results provide an integrated perspective on groundwater discharge which reflects the diffuse and widespread nature of SGD at this site.

Due to its 56 s half-life, the presence of any ^{220}Rn in a water column must indicate a very nearby source of thoron, and thus groundwater. Therefore, perhaps the best use of thoron might be as a prospecting tool for sites of significant groundwater outflows. At the Kahekili Beach Park submarine vents, the ^{220}Rn source stems from a prolonged buildup of radium by MnO$_2$ deposits that have precipitated as reducing groundwater becomes oxidized during discharge. This is similar to what Burnett et al. (2007b) observed in a New Jersey municipal water supply system where pipe scales effectively concentrated radium isotopes, thus producing a 'radon generator'. Chanyotha et al. (2014) used a similar RAD7 setup to prospect for ^{222}Rn and ^{220}Rn while underway in Bangkok canals and the analytical derivations to obtain thoron results presented here are identical. The thoron activities shown in Fig. 11 are based on three-point averages since the thoron RAD7 was set to 5-min cycles and the count rates were expectedly low. Assuming a low-tide mean ^{220}Rn activity ($n = 3$) of 82 ± 3 arbitrary units (arbitrary units are used here as the loss of ^{220}Rn during sampling is difficult to constrain) in discharging groundwater, inventories of ^{220}Rn over time are used to obtain an SGD rate of 101 cm d^{-1}, which equals a volumetric rate of 7070 m^3 d^{-1} if multiplied by the SGD-influenced area of Glenn et al. (2013). This ^{220}Rn-derived SGD rate is somewhat higher than the simultaneously derived ^{222}Rn SGD rate (87 ± 45 cm d^{-1}). This may reflect the much shorter integration time for thoron, which was confined here to just one low tide event. Also, in the radon model the mixing losses are estimated based on the negative net Rn fluxes. While this is inherently a conservative approach, the overall agreement between these two methods is good.

5. Conclusions

Recent studies have highlighted the disproportionately large rates of submarine groundwater emanating from volcanic islands (e.g. Garrison et al., 2003; Kim et al., 2003; Johnson et al., 2008; Street et al., 2008; Peterson et al., 2009; Cardenas et al., 2010; Huang et al., 2011; Swarzenski et al., 2013). This study utilized a combination of oceanographic-, thermal infrared imagery-, and ^{222}Rn and ^{220}Rn- time-series measurements, to study rates and scales of submarine groundwater discharge at a nearshore underwater vent site off west Maui, Hawaii. At this site, groundwater with a salinity as low as 3 is discharged into a coastal water column that is ~2 m deep. Sustained SGD at this site introduces terrestrially derived nutrient and trace elements, some of which are considerably elevated over ambient seawater values. SGD rates obtained in 2013 using thoron (101 cm d^{-1}) and radon (87 cm d^{-1}) compared favorably, considering the differences in the half-life of these two isotopes and the method assumptions. Oceanographic and thermal infrared imagery time-series analyses showed that discharge was modulated by tides and waves, and that mixing and advection of discharged groundwater also varied significantly with tides, winds, and waves. The combination of naturally occurring SGD tracers (^{222}Rn and ^{220}Rn) with a compliment of oceanographic time-series analyses provides new insight into how this coastal aquifer is connected to and interacts with the near-shore ocean.

Acknowledgments

References

Anderson, M.P., 2005. Heat as a groundwater tracer. Groundwater 43/6, 951–968.

Atkinson, et al., 2015. A multi-tracer approach to quantifying groundwater inflows to an upland river; assessing the influence of variable groundwater chemistry. Hydrol. Processes 29 (1), 1085–1099 http://dx.doi.org/10.1002/hyp.10122.

Bakalowicz, M., 2015. Karst and karst groundwater resources in the Mediterranean. Environ. Earth Sci. 74 (1), 5–14.

Banks, W.S.L., et al., 1996. Using thermal-infrared imagery to delineate groundwater discharge. Groundwater 24, 434–443.

Beck, A.J., et al., 2007. Radium mass-balance in Jamaica Bay, NY: evidence for a substantial flux of submarine groundwater. Mar. Chem. 106, 419–441 http://dx.doi.org/10.1016/j.marchem.2007.03.008.

Burnett, W.C., Dulaiova, H., 2003. Estimating the dynamics of groundwater input into the coastal zone via continuous radon-222 measurements. J. Environ. Radioact. 69, 21–35.

Burnett, W.C., et al., 2001. A continuous radon monitor for assessment of radon in coastal ocean waters. J. Radioanal. Nucl. Chem. 249, 167–172.

Burnett, W.C., et al., 2003. Groundwater and pore water inputs to the coastal zone. Biogeochemistry 66, 3–33.

Burnett, W.C., et al., 2006. Quantifying submarine groundwater discharge in the coastal zone via multiple methods. Sci. Total Environ. 367, 498–543.

Burnett, W.C., et al., 2007a. Remaining uncertainties in the use of Rn-222 as a quantitative tracer of submarine groundwater discharge. In: Sanford, W., Langevin, C., Polemio, M., Povinec, P. (Eds.), A New Focus on Groundwater–Seawater Interactions, 312. International Association of Hydrological Sciences Publication, pp. 109–118.

Burnett, W.C., et al., 2007b. Measuring thoron (^{220}Rn) in natural waters. In: Warwick, P. (Ed.), Environmental Radiochemical Analysis III. Royal Society of Chemistry, RSC Publishing, Cambridge, pp. 24–37.

Burnham, W.L., et al., 1977. Distribution of injected wastewater in the saline lava aquifer, Wailuku-Kahului wastewater treatment facility, Kahului, Maui, Hawaii. U.S. Geological Survey Open-File Report 77–469, 58 p.

Cartwright, I., Gilfedder, B., 2015. Mapping and quantifying groundwater inflows to Deep Creek (Maribyrnong catchment, SE Australia) using ^{222}Rn, implications for protecting groundwater-dependent ecosystems. Appl. Geochem. 52, 118–129, ISSN 0883-2927 http://dx.doi.org/10.1016/j.apgeochem.2014.11.020.

Cardenas, M.B., et al., 2010. Linking regional sources and pathways for submarine groundwater discharge at a reef by electrical resistivity tomography, 222Rn, and salinity measurements. Geophys. Res. Lett. 37, L16401, 10.1029/2010GL044066.

Chanyotha, et al., 2014. Prospecting for groundwater discharge in the canals of Bangkok via natural radon and thoron. J. Hydrol. 519, 1485–1492 http://dx.doi.org/10.1016/j.jhydrol.2014.09.014.

Charette, M.A., et al., 2008. Uranium-and thorium-series nuclides as tracers of submarine groundwater discharge. In: Krishnaswami, S., Cochran, J.K. (Eds.), U-Th Series Nuclides in Aquatic Systems. Elsevier, Amsterdam, pp. 155–192.

Constantz, J., et al., 2002. Analysis of temperature profiles for investigating stream losses beneath ephemeral channels. Water Resour. Res. 38 (12), 1–13.

Cooper, H. H., 1964. Sea water in coastal aquifers. United States Geological Survey Water Supply Paper 1613-C. Washington, D.C. 84 p.

Dailer, M.L., et al., 2008. Examining δ^{15}N values of intertidal macroalgae on Maui to identify locations and potential sources of nutrient enrichment, in Celia Smith, principal investigator. In: Integrated Ecosystem Management, Maui (Project Summary). University of Hawaii, Honolulu (accessed 4.11.09.) http://www.hawaii.edu/ssri/hcri/files/research/pdf/Smith-FY07-HCRI-NOAA-Report1.doc.

Dailer, M.L., et al., 2010. Using δ^{15}N values in algal tissue to map locations and potential sources of anthropogenic nutrient inputs on the island of Maui, Hawaii, USA. Mar. Pollut. Bull. 60, 655–671, http://dx.doi.org/10.1016/j.marpolbul.2009.12.021, ISSN 0025-326X.

Dailer, M.L., et al., 2012. Algal δ^{15}N values detect a wastewater effluent plume in nearshore and offshore surface waters and three dimensionally model the plume across a coral reef on Maui, Hawaii, USA. Mar. Pollut. Bullet. 64, 207–213.

Dimova, N.T., et al., 2012. Utilizing multi-channel electrical resistivity methods to examine the dynamics of the freshwater-saltwater interface in two Hawaiian groundwater systems. J. Geophys. Res. 117 (C02012), 12, http://dx.doi.org/10.1029/2011JC007509.

Dollar, S.J., Tribble, G.W., 1993. Recurrent storm disturbance and recovery: a long-term study of coral communities in Hawaii. Coral Reefs 12 (3), 223–233, http://dx.doi.org/10.1007/bf00334481.

Dollar, S., Andrews, C., 1997. Algal blooms off west Maui—assessing causal linkages between land and the coast ocean, Final Report for National Oceanic and Atmospheric Administration Coastal Ocean Program Office and University of Hawaii Sea Grant College Program, Honolulu, HI.

Dollar, S.J., et al., 1999. Investigation the relationship between cesspool nutrients and abundance of Hypnea musciformis in West Maui, Hawaii, Report State of Hawaii Department of Health, Honolulu, Hawaii.

Duarte, T.K., et al., 2006. Assessment of submarine groundwater discharge by handheld aerial infrared imagery: case study of Kaloko fishpond and bay, Hawaii. Limnol. Oceanogr. Methods 4, 227–236.

Dulaiova, H., et al., 2006. Assessment of groundwater discharges into West Neck Bay, New York, via natural tracers. Cont. Shelf Res. 26, 1971–1983.

Engott, J.A., Vana, T.T., 2007. Effects of agricultural land-use changes and rainfall on ground-water recharge in Central and West Maui, Hawaii, 1926–2004, U.S. Geological Survey Scientific Investigations Report 2007–5103, 56p.

Evenhuis, C., et al., 2015. Modelling coral calcification accounting for the impacts of coral bleaching and ocean acidification. Biogeosciences 12, 2607–2630, http://dx.doi.org/10.5194/bg-12-2607-2015.

Ferguson, G., Gleeson, T., 2012. Vulnerability of coastal aquifers to groundwater use and climate change. Nat. Clim. Change 2, 342–345, http://dx.doi.org/10.1038/nclimate1413.

Fleury, P., et al., 2007. Submarine springs and coastal karst aquifers: s review. J. Hydrol., 79–92, http://dx.doi.org/10.1016/j.jhydrol.2007.03.009, ISSN 0022-1694.

Garrison, G.H., et al., 2003. Measurement of submarine groundwater discharge in Kahana Bay, Oahu, Hawaii. Limnol. Oceanogr. 48, 920–928.

Giambelluca, T.W., et al., 1986. Rainfall atlas of Hawaii: State of Hawaii, Department of Land and Natural Resources, Division of Water and Land Development, Report R76, pp. 267.

Gingerich, S.B., 2008. Ground-water availability in the Wailuku area, Maui, Hawaii, U.S. Geological Survey Scientific Investigations Report 2008–5236, 95p.

Gingerich, S.B., Voss, C.I., 2005. Three-dimensional variable-density flow simulation of a coastal aquifer in southern Oahu, Hawaii, USA. Hydrogeol. J. 13, 436–450.

Gingerich, S.B., Engott, J.A., 2012. Groundwater availability in the Lahaina District, West Maui, Hawaii, U.S. Geological Survey Scientific Investigations Report 2012–5010, 90 p.

Glenn, C.R., et al., 2012. Lahaina groundwater tracer study—Lahaina, Maui, Hawai'i, Final Interim Report. Prepared from the State of Hawaii Department of Health, the U.S. Environmental Protection Agency, and the U.S. Army Engineer Research and Development Center. http://www.epa.gov/region9/water/groundwater/uic-pdfs/lahaina02/lahaina-final-interim-report.pdf.

Glenn, C.R., et al., 2013. Lahaina groundwater tracer study—Lahaina, Maui, Hawai'i, Final Report. Prepared from the State of Hawaii Department of Health, the U.S. Environmental Protection Agency, and the U.S. Army Engineer Research and Development Center. http://www.epa.gov/region9/water/groundwater/uic-pdfs/lahaina02/lahaina-gw-tracer-study-final-report-june-2013.pdf.

Gonneea, M.E., et al., 2014. Trace element geochemistry of groundwater in a karst subterranean estuary (Yucatan Peninsula, Mexico). Geochim. Cosmochim. Acta 132, 31–49.

Grubert, E.A., Webber, W.E., 2015. Energy for water and water for energy on Maui Island, Hawaii. Environ. Res. Lett. 10, 064009, http://dx.doi.org/10.1088/1748-9326/10/6/064009.

Horn, D.P., 2006. Measurements and modeling of beach groundwater flow in the swash-zone: a review. Cont. Shelf Res. 26, 622–652, http://dx.doi.org/10.1016/j.csr.2006.02.001.

Huang, K.-F., et al., 2011. Nonhomogeneous seawater Sr isotopic composition in the coastal oceans: A novel tool for tracing water masses and submarine groundwater discharge. Geochem. Geophys. Geosyst. 12, http://dx.doi.org/10.1029/2010GC003372.

Hunt, C.D.,Jr., Rosa, S.N., 2009. A multitracer approach to detecting wastewater plumes from municipal injection wells in nearshore marine waters at Kihei and Lahaina, Maui, Hawaii: U.S. Geological Survey Scientific Investigations Report 2009–5253, 166 p., http://pubs.usgs.gov/sir/2009/5253/ (accessed 17.2.12.).

Hunt, C.D.,Jr., 2007. Ground-water nutrient flux to coastal waters and numerical simulation of wastewater injection at Kihei, Maui, Hawaii: U.S. Geological Survey Scientific Investigations Report 2006–5283, 69 p.

Johnson, A.G., et al., 2008. Aerial infrared imaging reveals large nutrient-rich groundwater inputs to the ocean. Geophys. Res. Lett. 35, L15606, http://dx.doi.org/10.1029/2008GL034574.

Johnson, A.G., et al., 2014. Spatially distributed groundwater recharge estimated using a water-budget model for the Island of Maui, Hawaii, 1978–2007: U.S. Geological Survey Scientific Investigations Report 2014–5168, 53 p.

Kelly, J.L., et al., 2013. High-resolution aerial infrared mapping of groundwater discharge to the coastal ocean. Limnol. Oceanogr. Methods 11 (5), 262–277.

Ketabchi, H., Behzad, A., 2015. Review: coastal groundwater optimizationadvances, challenges, and practical solutions. Hydrogeol. J., 1–26, http://dx.doi.org/10.1007/s10040-015-1254-1.

Kim, G., et al., 2003. Large submarine groundwater discharge (SGD) from a volcanic island. Geophys. Res. Lett. 30 (21), 2098, http://dx.doi.org/10.1029/2003GL018378.

Kim, G., et al., 2011. Submarine groundwater discharge from oceanic islands standing in oligotrophic oceans: implications for global biological production and organic carbon fluxes. Limnol. Oceanogr. 56 (2), 673–682, http://dx.doi.org/10.4319/lo.2011.56.2.0673.

Langenheim, V.A.M., Clague, D.A., 1987. The Hawaiian Emperor volcanic chain, Part II, Stratigraphic framework of volcanic rocks of the Hawaiian Island, Chap. 1 of Decker, R.W., Wright, T.L., Stauffer, P.H.,(Eds.), Volcanism in Hawaii: U.S. Geological Survey Professional Paper 1350, vol. 1, p. 55–84.

Li, L., et al., 1999. Submarine groundwater discharge and associated chemical input to a coastal sea. Water Resour. Res. 35, 3253–3259, http://dx.doi.org/10.1029/1999WR900189.

Moon, D.S., et al., 2003. Preconcentration of radium isotopes from natural waters using MnO_2 Resin. Appl. Radiat. Isot. 4, 255–262, 00193-3 ISSN 0969-8043 http://dx.doi.org/10.1016/S0969-8043(03).

Moore, W.S., 2010. The effect of submarine groundwater discharge on the ocean. Annu. Rev. Mar. Sci. 2, 59–88, http://dx.doi.org/10.1146/annurev-marine-120308-081019.

Niswonger, R.G., Prudic, D.E., 2003. Modeling heat as a tracer to estimate streambed seepage and hydraulic conductivity. In: Stonestrom, D.A., Constantz, J. (Eds.), Heat as a Tool for Studying the Movement of Ground Water Near Streams. Reston, Virginia, pp. 81–89, USGS Circular 1260.

Ortega, L., et al., 2015. Using ^{222}Rn to identify and quantify groundwater inflows to the Mundo River (SE Spain). Chem. Geol. 395, 67–79 http://dx.doi.org/10.1016/j.chemgeo.2014.12.002.

Parra, S.M., et al., 2015. Salt intrusion at a submarine spring in a fringing reef lagoon. J. Geophys. Res. Oceans 120, http://dx.doi.org/10.1002/2014JC010459.

Peterson, R.N., et al., 2009. Quantification of point-source groundwater discharges from the shoreline of the Big Island, Hawaii. Limnol. Oceanogr. 54, 890–904.

Prouty, N.G., et al., 2016. Compounding effects of contaminated groundwater on coral reef health. Estuarine Coastal Shelf Sci., In review.

Rodellas, V., et al., 2015a. The influence of sediment sources on radium-derived estimates of submarine groundwater discharge. Mar. Chem. 171, 107–117, http://dx.doi.org/10.1016/j.marchem.2015.02.010.

Rodellas, V., et al., 2015b. Submarine groundwater discharge as a major source of nutrients to the Mediterranean Sea. PNAS 112, 3926–3930, http://dx.doi.org/10.1073/pnas.1419049112.

Rotzoll, K., Fletcher, C., 2013. Assessment of groundwater inundation as a consequence of sea-level rise. Nat. Climate Change 5, 477–481 http://dx.doi.org/10.1038/nclimate1725.

Rotzoll, K., et al., 2010. Changes of freshwater-lens thickness in basaltic islands aquifers overlain by thick coastal sediments. Hydrogeol. J. 18/6, 1425–1436.

Schubert, M., et al., 2012. Air-water partitioning of 222Rn and its dependence on water temperature and salinity. Environ. Sci. Technol. 46, 3905–3911.

Santos, I.R., et al., 2012. The driving forces of porewater and groundwater flow in permeable coastal sediments: a review. Estuarine Coastal Shelf Sci. 98, 1–15 http://dx.doi.org/10.1016/j.ecss.2011.10.024.

Shade, P.J., 1996. Water budget for the Lahaina district, island of Maui, Hawaii, Water Resources Investigations Report 96–4238, 27p.

Slomp, C.P., Van Cappellen, P., 2004. Nutrient inputs to the coastal ocean through submarine groundwater discharge: controls and potential impact. J. Hydrol. 295, 64–86, http://dx.doi.org/10.1016/j.jhydrol.2004.02.018.

Smith, J.E., et al., 2005. Characterization of a large-scale ephemeral bloom of the green alga *Cladophora sericea* on the coral reefs of West Maui Hawaii. Mar. Ecol. Prog. Ser. 302, 77–91.

Soicher, A.J., Peterson, F.L., 1997. Terrestrial nutrient and sediment fluxes to the coastal waters of west Maui, Hawaii. Pac. Sci. 51, 221–232.

Souza, W.R., 1981. Ground-water status report, Lahaina District, Maui, Hawaii, 1980, U.S. Geological Survey Open-File Report 81–549, 2 map sheets.

Storlazzi, C.D., Field, M.E., 2008. Winds, waves, tides, and the resulting flow patterns and fluxes of water, sediment, and coral larvae off West Maui, Hawaii. USGS Open-File Report 2008–1215, 13p. http://pubs.usgs.gov/of/2008/1215/.

Storlazzi, C.D., Jaffe, B.E., 2008. The relative contribution of processes driving variability in flow, shear, and turbidity over a fringing coral reef: West Maui, Hawaii. Estuarine Coastal Shelf Sci. 77 (4), 549–564.

Storlazzi, C.D., McManus, M.A., Logan, J.B., McLaughlin, B.E., 2006. Cross-shore velocity shear, eddies, and heterogeneity in water column properties over fringing coral reefs: West Maui, Hawaii. Cont. Shelf Res. 26, 401–421.

Strauch, A.M., et al., 2015. Climate driven changes to rainfall and streamflow patterns in a model tropical island hydrological system. J. Hydrol. 523, 160–169, ISSN 0022–1694 http://dx.doi.org/10.1016/j.jhydrol.2015.01.045.

Street, J.H., et al., 2008. Submarine groundwater discharge and nutrient addition to the coastal zone and coral reefs of leeward Hawai'i. Mar. Chem. 109, 355–376, http://dx.doi.org/10.1016/j.marchem.2007.08.009.

Stearns, H.T., Macdonald, G.A., 1942. Geology and groundwater resources of the island of Maui, Hawaii. Hawaii Div. Hydrogr. Bull. 7, 344.

Swarzenski, P.W., 2007. U/Th series radionuclides as tracers of coastal groundwater. Chem. Rev. 107 (2), 663–674, http://dx.doi.org/10.1021/cr0503761.

Swarzenski, P.W., Kindinger, J.L., 2003. Leaky coastal margins: examples of enhanced coastal groundwater/surface water exchange from Tampa Bay and Crescent Beach Submarine Spring, Florida, USA. In: Cheng, A., Ouazar, D. (Eds.), Coastal Aquifer Management, Monitoring and Modeling and Case Studies. CRC/Lewis Press, pp. 93–112.

Swarzenski, P.W., Izbicki, J.A., 2009. Examining coastal exchange processes within a sandy beach using geochemical tracers, seepage meters and electrical resistivity. Estuarine Coastal Shelf Sci. 83, 77–89, http://dx.doi.org/10.1016/j.ecss.2009.03.027.

Swarzenski, P.W., et al., 2001. Using multiple geochemical tracers to characterize the hydrogeology of the submarine spring off Crescent Beach, Florida. Chem. Geol. 179, 187–202, http://dx.doi.org/10.1016/s0009-2541(01) 00322-9.

Swarzenski, P.W., et al., 2006. Combined time-series resistivity and geochemical tracer techniques to examine submarine groundwater discharge at Dor Beach, Israel. Geophys. Res. Lett. 33, L24405, http://dx.doi.org/10.1029/2006GL028282.

Swarzenski, P.W., et al., 2007. A geochemical and geophysical examination of submarine groundwater discharge and associated nutrient loading estimates into Lynch Cove, Hood Canal, WA. Environ. Sci. Technol. 41, 7022–7029, http://dx.doi.org/10.1021/es070881a.

Swarzenski, P.W., et al., 2012. Nearshore morphology, benthic structure, hydrodynamics, and coastal groundwater discharge near Kahekili Beach Park, Maui, Hawaii, U.S. Geological Survey Open-File Report 2012–1166, 34p.

Swarzenski, P.W., et al., 2013. A geochemical and geophysical assessment of coastal groundwater discharge at select sites in Maui and Oahu, Hawaii. In: Wetzelhuetter, C. (Ed.), Groundwater in the Coastal Zones of Asia Pacific. Springer, pp. 27–46, http://dx.doi.org/10.1007/978-94-007-5648-9.

Taniguchi, M., 1993. Evaluation of vertical groundwater fluxes and thermal properties of aquifers based on transient temperature-depth profiles. Water Resour. Res. 29 (7), 2021–2026.

Taniguchi, M., et al., 2003. Evaluations of groundwater discharge rates from subsurface temperature in Cockburn Sound, Western Australia. Biogeochemistry 66 (1–2), 111–124.

Tovar-Sanchez, A., et al., 2014. Contribution of groundwater discharge to the coastal dissolved nutrients and trace metal concentrations in Majorca Island: karstic vs detrital systems. Environ. Sci. Technol. 48, 11819–11827 http://dx.doi.org/10.1021/es502958t.

Vallejos, A., et al., 2015. Processes influencing groundwater level and the freshwater-saltwater interface in a coastal aquifer. Water Resour. Manag. 29 (3), 679–697, http://dx.doi.org/10.1007/s11269-014-0621-3.

Vega-Thurber, R.L., et al., 2014. Chronic nutrient enrichment increases prevalence and severity of coral disease and bleaching. Global Change Biol. 20, 544–554.

Zhang, H., Sheng, J., 2015. Examination of extreme sea levels due to storm surges and tides over the northwest Pacific Ocean. Cont. Shelf Res. 93, 81–97 http://dx.doi.org/10.1016/j.csr.2014.12.001.